



Ultrasonic-assisted fabrication of metallic glass composites

Y. Zhang^{a,b,1}, H. Zhao^{b,c,1}, Y.Q. Yan^b, X. Tong^b, J. Ma^{a,*}, H.B. Ke^{b,*}, W.H. Wang^{b,c}

^a Shenzhen Key Laboratory of High Performance Nontraditional Manufacturing, College of Mechatronics and Control Engineering, Shenzhen University, Room 801, Shenzhen 518060, People's Republic of China

^b Songshan Lake Materials Laboratory, Dongguan 523808, People's Republic of China

^c School of Physics, Liaoning University, Shenyang 110036, People's Republic of China

ARTICLE INFO

Keywords:

Metallic glass composite
Ultrasonic vibration
Tailorable properties

ABSTRACT

Metallic glass composites (MGCs) inherit the high strength of their glassy matrix and exhibit remarkable plastic deformation, hence have great potential in engineering applications. However, their preparation often relays on arduous component exploration or involves elusive technological process. Here, we report a facile route to fabricate MGC using ultrasonic vibration (UV) and the fabrication process can be manually controlled. By appropriately modulating the amplitude and time of UV, the MGCs with different proportion of crystalline phase can be obtained readily and accurately in seconds under low-pressure at room temperature owing to the unique soften behavior of MG under UV. The deformation behavior and the hardness were evaluated using nano-indentation testing, demonstrating better ductility when compared with the as-cast sample and reduced hardness for the MGCs as increased proportion of crystalline phase. These results may provide a new approach for the rapid and controllable fabrication of MGCs with designed properties.

1. Introduction

Metallic glasses (MGs), inheriting the disorder structure from their melts during the rapid quenching process, possess excellent mechanical properties when compared with their corresponding crystalline counterparts [1–8]. However, owing to the lack of defects such as dislocations to dissipate energy during deformation, MGs fail in an apparently brittle manner because of localized shear bands formation in unconstrained loading geometries [9,10]. To overcome this trade-off, MG composites (MGCs) emerge as derivative materials with both high strength and considerable plasticity [11–13]. The inhomogeneous microstructure with isolated second crystalline phase in a MG matrix stabilizes the glass against the catastrophic failure associated with unlimited extension of shear bands, resulting in enhanced global plasticity and more graceful failure. Thus, MGCs have been a hot research topic in past decades and have great potential in engineering application as structural materials [14–17].

Generally speaking, there are three approaches to prepare MGCs with a mixed microstructure of MG matrix and a second crystalline phase. The first one is to add a second phase particles prior to casting, also called “*ex-situ*” composites [11,13,18–23]. It is common to produce

MG composites by casting of a glass-forming alloy around a preform of crystalline particles or fibers, or making amorphous/crystalline laminates [24]. For example, Choi-Yim and Johnson synthesized MGCs by intruding both ceramics and metals as reinforcement into the metallic glass matrix while keep the matrix amorphous even after adding up to a 30 vol% fraction of particles or wires [13]. The second one is to directly generate the “*in-situ*” composites through precipitation of a crystalline phase during solidification with the remainder of the melt forming a glass [12,25–27]. Recently, the Zr/Ti based MGCs containing β -Zr/Ti phases and CuZr-based MGCs containing B2 CuZr phases were successfully fabricated and exhibited a novel plastic deformation mechanism under tension [28]. The third one is to produce a nanocrystalline phase in the matrix through partial devitrification of a MG [29–33]. It was found that the dispersion of nanocrystals only a few nanometers in diameters in an amorphous matrix can lead to an increase of both strength and ductility in $Zr_{53}Ti_5Ni_{10}Cu_{20}Al_{12}$ [29]. Nevertheless, it is tedious and time-consuming to fabricate the “*ex-situ*” or “*in-situ*” MG composites due to the requirement of vast composition exploration as well as elusive technological process [34]. Although partial devitrification is a relatively handy approach, it still needs complicated heat treatment [35,36]. Thus, a new rapid and controllable preparation method to obtain MG

* Corresponding authors.

E-mail addresses: majiang@szu.edu.cn (J. Ma), kehaibo@sslslab.org.cn (H.B. Ke).

¹ These authors contributed equally to this work.

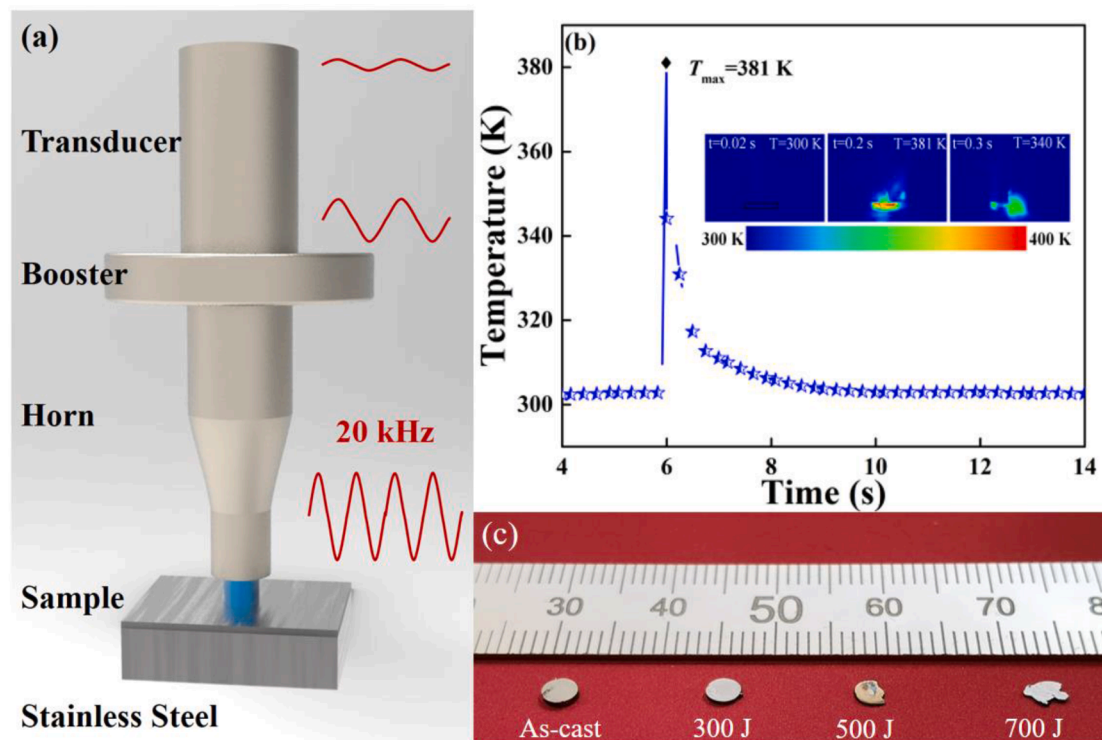


Fig. 1. Schematic diagram of ultrasonic treatment process and the appearances of as-cast and UV processed samples. (a) Sketch of ultrasonic vibration procedure, a high frequency ultrasonic vibration of 20 kHz is applied to the sample through the horn. (b) The temperature evolution detected by high precision infrared thermometer during ultrasonic vibration process with UV energy of 700 J. (c) Comparison of the overall morphology of the as-cast sample and the processed MGs.

composites is urgently needed.

Recently, an ultrasonic-assisted forming method has been employed to fabricate multiphase MGs [37–39]. By using high-frequency vibration, two originally separated amorphous alloys can be bonded together well at the temperature below T_g [37], also micro- to nano-structure can be fabricated on the surface of amorphous alloys [38,40]. It is noteworthy that ultrastability of supercooled liquid can be efficiently realized by ultrasonic induced atomic rearrangement [39]. In this work, we proposed a facile route to fabricate La-based MGC through ultrasonic vibration. By appropriately modulating the amplitude and time of UV, the MGs with different proportion of crystalline phase can be obtained readily and accurately in seconds under low-pressure at room temperature owing to the unique soften behavior of MG under UV. The deformation behavior and hardness of these composite materials were evaluated by nanoindentation test and the indentation morphology of specimens were observed by AFM. The underlying physics of the formation process of crystalline in MG matrix is also discussed.

2. Materials and methods

The alloy ingots with normal composition of $\text{La}_{64}\text{Al}_{14}\text{Cu}_{22}$ with a mixture of elements with a purity of at least 99.9% were prepared by arc melting method under a Ti-gettered high-purity argon atmosphere. Each ingot was remelted five times to make sure a homogeneous composition. A cylindrical rod with diameter of 3 mm was prepared with copper-mold suction. Disks with thickness of 1 mm were cut by diamond saw and polished to ensure parallel of the top and bottom sides. Whereafter the polished samples were treated by ultrasonic vibration equipment. The equipment consists of three important mountings (see in Fig. 1a). A transducer for converting electrical energy to mechanical vibration, a booster for amplifying the amplitude of vibrations and a horn to transfer mechanical vibrations to the specimens. A low loading of 10 Newton was preloaded to make sure the closely contact between the samples and the horn. Then various energy from 100 J to 700 J was applied to the

samples within seconds. In order to monitor the thermal effect during the process, an infrared instrument with high precision of 1 K was used to obtain the temperature changes. In order to further test the phase structure changes of the specimens before and after the UV process, the X-ray diffraction (XRD, Bruke D8-ADVANCE) with $\text{Cu } \alpha$ radiation was employed. The thermal response was confirmed by differential scanning calorimetry (DSC, PE-DSC 8000) at a heating rate of 20 K/min. Different heating rate including 10, 20, 40, 60 K/min were used for measuring the activation energy of crystallization process. The hardness were tested by nanoindentation apparatus (Bruker TI 980, Germany) with a Berkovich tip, applying a maximum loading of 3 mN with a loading rate of 0.5 mNs^{-1} . At least 10 indentation tests were carried out for each sample to obtain the average value. In order to observe the deformation behavior after indentation, the indent morphology was subsequently observed by atomic force microscopy (AFM, Bruker Icon). The AFM imaging was acquired in tapping mode using probe Tap300 Al-G (Budget Sensors) with a resonant frequency of 300 kHz. Beside, in order to confirm the formation of second phases and compare their distribution after UV process, the surface topographies were observed by field emission scanning electron microscopy (SEM; Gemini Sigma 300) using back scattering mode. Furthermore, specimens for transmission electron microscopy (TEM) measurement were prepared by the ion milling (PIPS II-695.c) with 3 keV ion beam energy at room temperature. Microstructures of the specimens were characterized by (TEM, JEOL JEM-2011F, 200 kV), and the selected area electron diffraction (SAED) was performed in TEM mode.

3. Results and discussion

The illustration of UV treatment is shown in Fig. 1a. Detailed information of UV equipment was introduced in above section. Due to the time of ultrasonic process which lasted for seconds, there may be some thermal effects on the samples. Fig. 1b shows the temperature profile during the whole UV process. It can be seen that the maximum

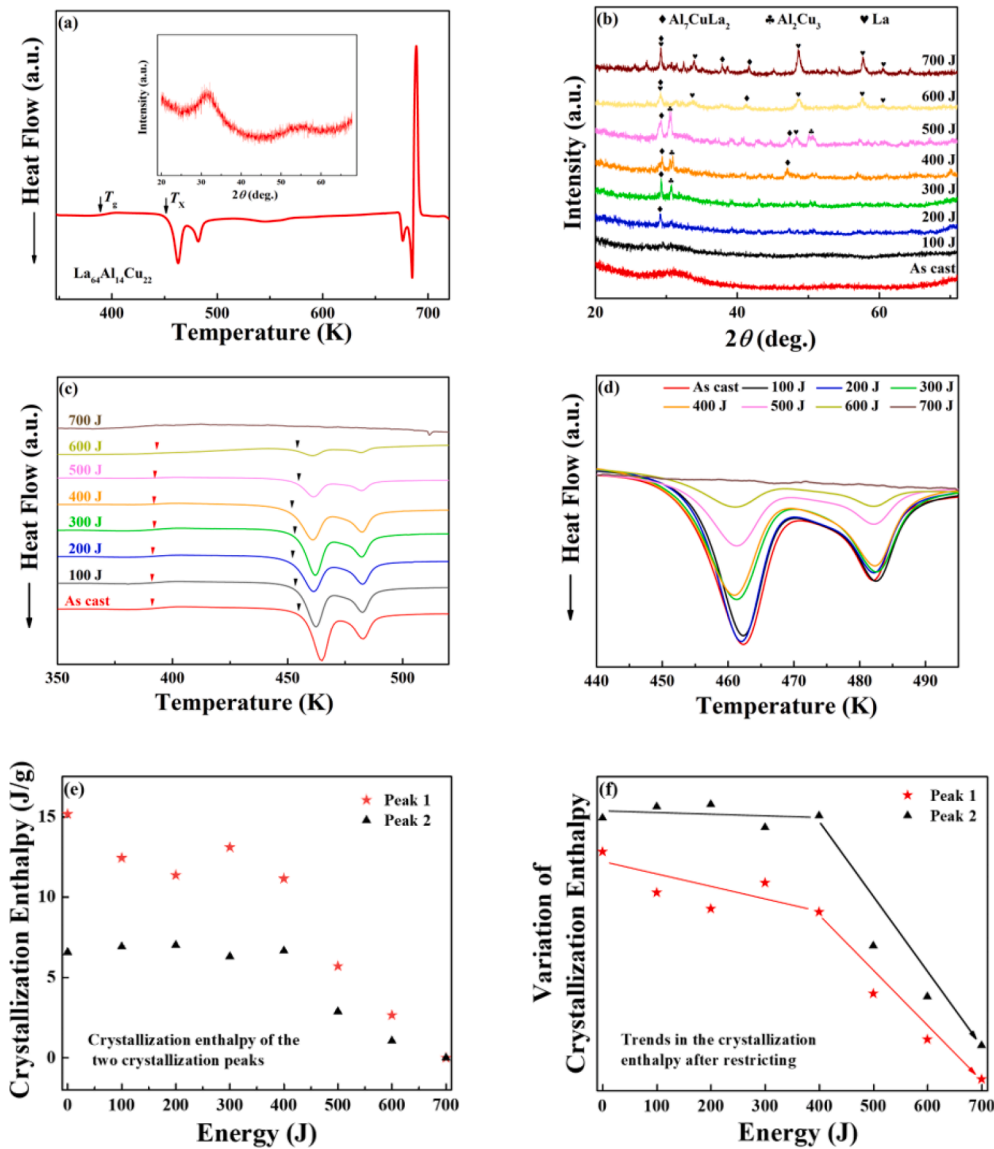


Fig. 2. The thermodynamic evolution behavior and intrinsic structural transform of La-based MG at diverse input energy. (a) The DSC trace of as-cast sample shows two independent exothermic peaks. The inset shows the XRD pattern with broad diffraction peak, indicating the completely amorphous state of as-cast sample. (b) XRD patterns of as-cast sample and processed samples, indicating that formation of the crystalline phases become more complex as the increasing of UV energy. (c) Comparison of DSC traces for as-cast and UV processed samples with various UV energies. (d) The enlarged DSC traces of crystallization peaks to highlight the transformations of crystallization peak and crystallization enthalpy with different samples. (e) The crystallization enthalpy versus UV input energy for two different peaks. (f) The variation of reduced crystallization enthalpy with UV input energy.

temperature in the whole process is 381 K for the input energy of 700 J, which is still below its T_g . Thus, the resulted soften behavior was not caused by temperature rise, which is similar to previous reports of UV process [39,41,42]. Fig. 1c displays the appearances of as-cast sample and the processed samples with different UV energy. Although the samples remain intact, obvious deformation can be observed when the UV energy increased to 700 J.

Fig. 2a shows the X-ray diffraction (XRD) and the differential scanning calorimetry (DSC) results of as-cast sample. It can be seen clearly that the as-cast sample consists of a broad diffraction peak, indicating the completely amorphous state. From the DSC trace, one can see that an endothermic glass transition ($T_g = 388$ K) followed by two exothermic crystallization events for as-cast sample. The onset crystallization transition temperature for the two peaks were $T_{x1} = 456$ K and $T_{x2} = 482$ K, independently, as well as the crystallization enthalpies were $\Delta H_{x1} = 14.7$ kJ/mol and $\Delta H_{x2} = 6.2$ kJ/mol, respectively. Fig. 2b shows the comparison of XRD patterns for as-cast and UV processed samples. Significant difference can be found in these XRD patterns. A broad diffraction peak indicating the completely amorphous state for as-cast sample. After UV process with 200 J, some sharp diffraction peaks begin to appear around 30° , which corresponding to the crystalline phase Al_7CuLa_2 . As the input energy exceed 400 J, more sharp

diffraction peaks can be found, indicating that more complex crystalline phase such as Al_7CuLa_2 , Al_2Cu_3 and La was formed. Thus, one can deduce that the samples have been processed into a kind of MGCs which contains different fraction of crystalline. In order to obtain the thermodynamics properties of these MGCs, Fig. 2c shows the comparison of DSC traces between as-cast and UV processed samples with a heating rate of 20 K/min. Except for the remarkable changes of the two crystallization exothermic peaks, no visible variation can be observed for both the T_g and T_x . The detail evolution of two crystallization peaks is displayed in the enlarged view (Fig. 2d). It can be found that both the two exothermic peaks decrease gradually as the input energy increase. As the UV energy reaching 700 J, the two peaks finally vanish implying the completely crystallization of the sample.

To investigate the structure evolution of these MGCs during the whole UV process, the variation of crystallization enthalpies with the UV energies was shown in Fig. 2e. We can find that there is a distinct two-stage downward tendency for the evolution of the crystallization enthalpy. Firstly, the enthalpy of the first exothermic peak is decreasing when the input energy is less than 400 J, while the second exothermic peak is almost unchanged. This behavior indicates that the structure transition from disorder to order under UV was extremely tardiness below 400 J. Afterwards, when the input energy exceeds 400 J, the

Table 1

Enthalpies of crystallization and crystalline phase contents of the MGCs corresponding to different ultrasonic energies.

UV energy (J)	ΔH_{x1} (J/g)	ΔH_{x2} (J/g)	ΔH (J/g)	Crystalline phase contents (%)
0	14.6	6.2	20.8	0
100	12.4	6.9	19.3	7.2
200	11.4	7.0	18.4	11.5
300	11.1	6.6	17.8	14.4
400	11.1	6.3	17.4	16.3
500	5.7	2.9	8.6	58.7
600	2.7	1.1	3.8	81.7
700	0	0	0	100

enthalpies of both two exothermic peaks decrease obviously, which imply that the ordering process under UV was rapid. Finally, both the areas of two crystallization peaks decreases to 0 J/g as the input energy increase to 700 J, which means the amorphous phase become crystalline completely. In addition, the crystalline phase content of the MGCs steadily rises with increasing ultrasonic energy, the specific values are shown in Table 1, where the crystalline phase content increases significantly when the energy is greater than 500 J. The MGCs completely crystallize when the energy hits 700 J.

To further understand the underlying physical mechanism, the activation energy of the two exothermic events was evaluated. Fig. 3a presents the DSC traces of as-cast specimens at different heating rates. As the heating rate increasing, T_{P1} and T_{P2} move to high temperature. The activation energy of the two crystallization peaks can be calculated by using the Kissinger model [43]. It expresses the dependence of T_{P1} and T_{P2} on the heating rate θ through the following equation $\ln\left(\frac{T^2}{\theta}\right) = \frac{E_c}{RT} + C$, where T is the temperature, R is the gas constant, E_c is activation energy and C is constant. Plotting of $\ln(T^2/\theta)$ versus $1000/T$, one can get the value of the activation energy E_c . As shown in Fig. 3b, the crystallization activation energy for the first event is 124.1 kJ/mol, which is significantly lower than that of the second event with 164.7 kJ/mol. These two different activation energies give an explanation for the phenomenon that different variation in crystallization enthalpies as the input UV energy increasing. Owing to the relatively low activation energy for the first peak, only part of atoms in the regions with loose packing can absorb the UV energy easily and rearrange into crystal phase gradually. Thus, the crystallization enthalpy of the first peak gradually reduces by 20% before 400 J while that of the second peak almost unchanged. Afterwards, as the applied UV energy exceed the overall crystallization activation energy, most of the activated atoms could across the energy barrier and reach to the stable crystalline state easily. As a consequence, the crystallization process of these MGCs would be accelerated. This also coincides with the aforementioned

two-stage downward tendency. That is, when the UV energy is less than 400 J, only the first exothermic peak is activated, so the crystallization enthalpy decreases tardily. Once it exceeds 400 J, both exothermic peaks are activated, resulting in a drastic decline in the crystallization enthalpy.

Fig. 4a-c display the evolution of surface morphology of as-cast sample and achieved MGCs. No crystalline phase can be observed in the as-cast sample (Fig. 4a). However, it can be seen that more and more dispersed second phases with size of several micrometers were formed in the amorphous matrix as the UV energy increase from 300 J to 500 J. Fig. 4d-f display the high-resolution TEM (HRTEM) images and the corresponding SAED patterns of as-cast specimen and MGCs. For as-cast sample (Fig. 4d), the diffractive halo-like SAED indicates the amorphous disordered atomic structure. However, with the UV energy of 300 J (Fig. 4e), some nanocrystalline structures are dispersed in the MG matrix, resulting in bright diffraction spots embedded in the diffraction halos. As shown in Fig. 4f, crystalline already occupy a large proportion when the UV energy reach 500 J, and bright spots in the multi-ring diffraction halos indicate complex crystallization products. In order to examine the mechanical properties of these MGCs, nanoindentation experiments were conducted. Fig. 4g shows the comparison of indentation morphology observed by AFM for as-cast sample and MGC obtained at 300 J. One can see obvious shear bands piling-ups around the indent of as-cast sample. However, a complete indent surround by smooth surface can be observed after process with UV energy of 300 J. The height profiles of the indents were characterized using the AFM lines scans, the smoother interface of the indent further proved that the formed MGC has better adaptability to deformation. It is known that the formation of dispersed nanocrystal in the glassy matrix could dissipate external energy to impede the rapid propagation of shear bands [44,45]. Thus, the ductility of the MGCs can be significantly enhanced when compared with that of as-cast MG.

In order to further learn the mechanical properties, the hardness of as-cast MG and MGCs were obtained according to the load-depth curve and the method of Oliver and Pharr. Fig. 4h shows the hardness of the MGCs processed with different input UV energy. It can be found that the hardness reduces a little bit when energy increase from 0 to 400 J and maintains a plateau between 100 J and 400 J. However, they decrease enormously (about 22%) when the input energy over 400 J as crystallization occurs over a large fraction of the samples. Generally, the hardness of a MG is higher than its counterpart crystalline as expected. We also notice that the changes of the hardness consistent with the variation of crystallization enthalpy, which demonstrated the reliability of these results. Therefore, through controlling the input UV energy, we can regulate the formation of crystalline phase in MGs by adjust the input energy in order to manipulate the hardness and young's modulus of MGCs. By this method, the MGCs with both high strength and

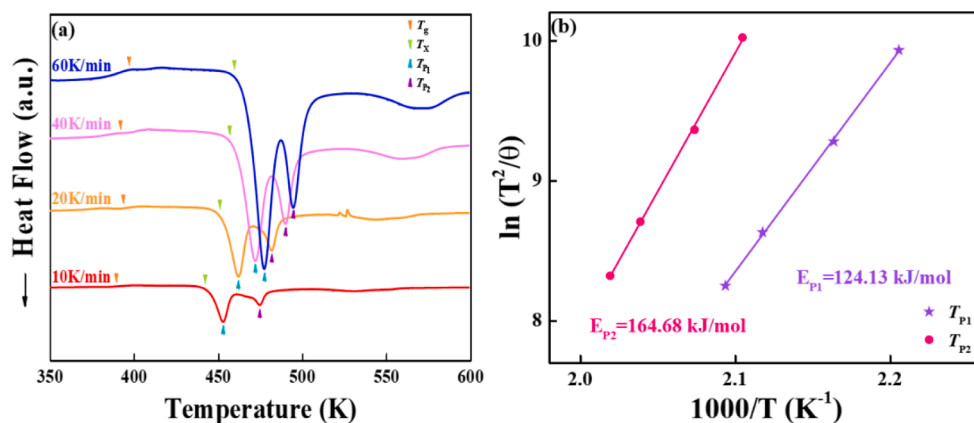


Fig. 3. The crystallization behavior of as-cast sample at different heating rates. (a) The changes of glass transition temperature (T_g) and the two crystallization peak temperatures (T_{P1} , T_{P2}) with heating rate. (b) Estimating the activation energies of two crystallization peaks using Kissinger equation.

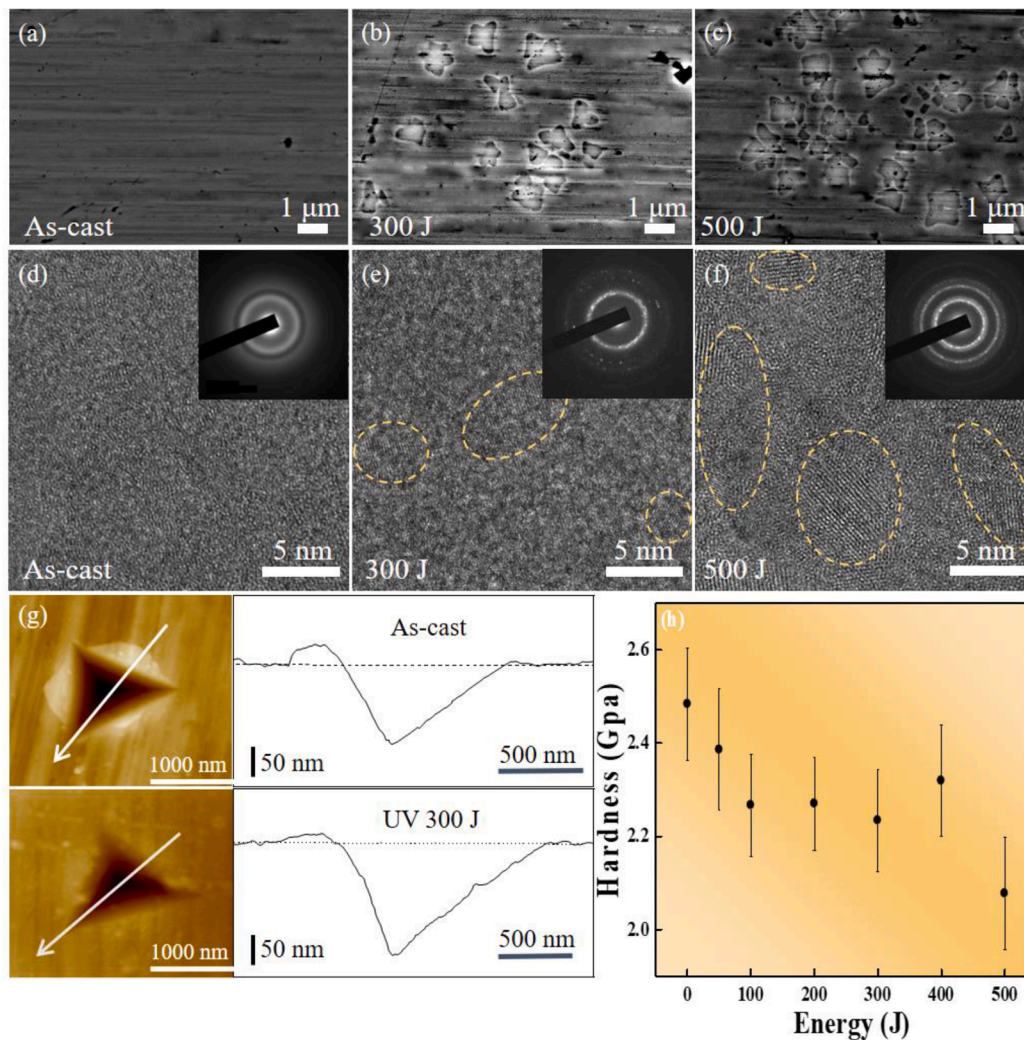


Fig. 4. The evolution of microstructure and hardness with ultrasonic vibration of as-cast MG and MGCs. (a)-(c) The evolution of microstructure of as-cast MG and MGCs, it can be seen that more dispersed second phases formed in the amorphous matrix as the increasing of UV energy. The scale bars in (a)-(c) are 1 μm. (d-f) HRTEM images of as-cast MG and MGCs, and the yellow dotted lines in (e) and (f) indicate the crystalline distribution in MGCs. Insets: SAED patterns taken from a large selected area. The scale bars in (d)-(f) are 5 nm. (g) The comparison of AFM topography around the indents between as-cast MG and MGC after nanoindentation testing. The lines in the AFM images indicated the traces where height profiles were taken. (h) The variation of hardness for MGCs with various UV energies (For interpretation of the references to color in this figure legend, the reader is referred to the web version of this article).

remarkable plasticity can be obtained in a certain UV energy range, so as to achieve the purpose of fleetly adjusting and controlling the composite phases of MGs.

4. Conclusions

In summary, through proper control the input energy of high-frequency ultrasonic vibration, we can success fabricate a series of MGCs in seconds under low-stress and at room temperature. The proportion of the crystalline phase of the MGCs can be readily and accurately modulated according to the UV energy. Due to the formation of dispersed second phases in the amorphous matrix, the MGC show ductile deformation behavior under nanoindentation when compared with as-cast state, also the hardness of these MGCs decreased gradually with increasing input energy. These results may offer a new approach for the rapid and quantitative control of the fabrication of MGCs. Also, combing with the advantages of ultrasonic molding, efficient manufacturing of precision component with MGCs may be easily be realized in the near future.

CRediT authorship contribution statement

Y. Zhang: Writing – original draft. **H. Zhao:** Conceptualization, Writing – original draft, Investigation. **Y.Q. Yan:** Formal analysis. **X. Tong:** Formal analysis. **J. Ma:** Supervision, Resources, Writing – review & editing. **H.B. Ke:** Supervision, Resources, Writing – review & editing. **W.H. Wang:** Writing – review & editing.

Declaration of Competing Interest

The authors declare that no conflict of interest or personal relationships that could have influenced the work reported in this letter. All the authors listed have approved the manuscript that is enclosed.

Data availability

Data will be made available on request.

Acknowledgments

This work was supported by Guangdong Major Project of Basic and Applied Basic Research, China [Grant No. 2019B030302010]; the National Key Research and Development Program of China [Grant No. 2018YFA0703604]; the National Natural Science Foundation of China [Grant No. 52071222, 51871157]; the Guangdong Basic and Applied Basic Research Foundation, China [Grant No. 2019B1515130005]; and the Strategic Priority Research Program of the Chinese Academy of Sciences [Grant No. XDB30000000].

References

- W. Klement, R.H. Willens, P. Duwez, Non-crystalline structure in solidified gold-silicon alloys, *Nature* 187 (1960) 869–870, <https://doi.org/10.1038/187869b0>.
- J. Hafner, Theory of the formation of metallic glasses, *Phys. Rev. B* 21 (1980) 406–426, <https://doi.org/10.1103/PhysRevB.21.406>.
- H. Chen, Y. He, G.J. Shiflet, S.J. Poon, Mechanical properties of partially crystallized aluminum based metallic glasses, *Scr. Metall. Mater.* 25 (1991) 1421–1424, [https://doi.org/10.1016/0956-716X\(91\)90426-2](https://doi.org/10.1016/0956-716X(91)90426-2).
- M.F. Ashby, A.L. Greer, Metallic glasses as structural materials, *Scr. Mater.* 54 (2006) 321–326, <https://doi.org/10.1016/j.scriptamat.2005.09.05>.
- J. Dong, Y. Huan, B. Huang, J. Yi, Y.H. Liu, B.A. Sun, W.H. Wang, H.Y. Bai, Unusually thick shear-softening surface of micrometer-size metallic glasses, *Innovation* 2 (2021), 100106, <https://doi.org/10.1016/j.xinn.2021.100106>.
- H. Li, Z. Li, J. Yang, H.B. Ke, B. Sun, C.C. Yuan, J. Ma, J. Shen, W.H. Wang, Interface design enabled manufacture of giant metallic glasses, *Sci. China Mater.* 64 (2021) 964–972, <https://doi.org/10.1007/s40843-020-1561-x>.
- J. Zhou, Q. Wang, X. Hui, Q. Zeng, Y. Xiong, K. Yin, B. Sun, L. Sun, M. Stoica, W. Wang, B. Shen, A novel FeNi-based bulk metallic glass with high notch toughness over 70 MPa m^{1/2} combined with excellent soft magnetic properties, *Mater. Des.* 191 (2020), <https://doi.org/10.1016/j.matdes.2020.108597>.
- J. Zhou, Q. Wang, Q. Zeng, K. Yin, A. Wang, J. Luan, L. Sun, B. Shen, A plastic FeNi-based bulk metallic glass and its deformation behavior, *J. Mater. Sci. Technol.* 76 (2021) 20–32, <https://doi.org/10.1016/j.jmst.2020.11.016>.
- A.L. Greer, Y.Q. Cheng, E. Ma, Shear bands in metallic glasses, *Mater. Sci. Eng. R* 74 (2013) 71–132, <https://doi.org/10.1016/j.mser.2013.04.001>.
- X.K. Xi, D.Q. Zhao, M.X. Pan, W.H. Wang, Y. Wu, J.J. Lewandowski, Fracture of brittle metallic glasses, *Phys. Rev. Lett.* 94 (2005), 125510, <https://doi.org/10.1103/PhysRevLett.94.125510>.
- Y.K. Xu, M. Han, X. Jian, E. Ma, Mg-based bulk metallic glass composites with plasticity and gigapascal strength, *Acta Mater.* 53 (2005) 1857–1866, <https://doi.org/10.1016/j.actamat.2004.12.036>.
- D.C. Hofmann, J.Y. Suh, A. Wiest, G. Duan, M.L. Lind, M.D. Demetriou, W. L. Johnson, Designing metallic glass matrix composites with high toughness and tensile ductility, *Nature* 451 (2008) 1085–1089, <https://doi.org/10.1038/nature06598>.
- H. Choi-Yim, W.L. Johnson, Bulk metallic glass matrix composites, *Appl. Phys. Lett.* 71 (1997) 3808–3810, <https://doi.org/10.1063/1.120512>.
- Z.P. Chen, J.E. Gao, Y. Wu, H. Wang, X.J. Liu, Z.P. Lu, Designing novel bulk metallic glass composites with a high aluminum content, *Sci. Rep.* 3 (2013) 3353, <https://doi.org/10.1038/srep03353>.
- D.K. Balch, E. Üstündag, D.C. Dunand, Elasto-plastic load transfer in bulk metallic glass composites containing ductile particles, *Metall. Mater. Trans. A* 34A (2003) 1787, <https://doi.org/10.1007/s11661-003-0145-6>.
- P. Gargarella, S. Pauly, K.K. Song, J. Hu, N.S. Barekar, M. Samadi Khoshkhou, A. Teresiak, H. Wendrock, U. Kühn, C. Ruffing, E. Kerscher, J. Eckert, Ti-Cu-Ni shape memory bulk metallic glass composites, *Acta Mater.* 61 (2013) 151–162, <https://doi.org/10.1016/j.actamat.2012.09.042>.
- D.C. Hofmann, Shape memory bulk metallic glass composites, *Science* 329 (2010) 1294–1295, <https://doi.org/10.1126/science.1193522>.
- M. Kinaka, H. Kato, M. Hasegawa, A. Inoue, High specific strength Mg-based bulk metallic glass matrix composite highly ductilized by Ti dispersoid, *Mater. Sci. Eng. A* 494 (2008) 299–303, <https://doi.org/10.1016/j.msea.2008.04.039>.
- H. Choi-Yim, R. Busch, U. Köster, W.L. Johnson, Synthesis and characterization of particulate reinforced Zr₅₇Nb₅Al₁₀Cu_{15.4}Ni_{12.6} bulk metallic glass composites, *Acta Mater.* 47 (1999) 2455–2462, [https://doi.org/10.1016/S1359-6454\(99\)00103-2](https://doi.org/10.1016/S1359-6454(99)00103-2).
- R.B. Dandliker, R.D. Conner, W.L. Johnson, Melt infiltration casting of bulk metallic-glass matrix composites, *J. Mater. Res.* 13 (1998) 2896–2901, <https://doi.org/10.1557/JMR.1998.0396>.
- R.D. Conner, R.B. Dandliker, W.L. Johnson, Mechanical properties of tungsten and steel fiber reinforced Zr_{41.25}Ti_{13.75}Cu_{12.5}Ni₁₀Be_{22.5} metallic glass matrix composites, *Acta Mater.* 46 (1998) 6089–6102, [https://doi.org/10.1016/S1359-6454\(98\)00275-4](https://doi.org/10.1016/S1359-6454(98)00275-4).
- X. Liang, X. Zhu, X. Li, R. Mo, Y. Liu, K. Wu, J. Ma, High-entropy alloy and amorphous alloy composites fabricated by ultrasonic vibrations, *Sci. China Phys. Mech. Astron.* 63 (2020), 116111, <https://doi.org/10.1007/s11433-020-1560-4>.
- J. Fu, J. Yang, K. Wu, H. Lin, W. Wen, W. Ruan, S. Ren, Z. Zhang, X. Liang, J. Ma, Metallic glue for designing composite materials with tailorable properties, *Mater. Horiz.* 8 (2021) 1690–1699, <https://doi.org/10.1039/d1mh00521a>.
- Z.Q. Chen, M.C. Li, J.S. Cao, F.C. Li, S.W. Guo, B.A. Sun, H.B. Ke, W.H. Wang, Interface dominated deformation transition from inhomogeneous to apparent homogeneous mode in amorphous/amorphous nanolaminates, *J. Mater. Sci. Technol.* 99 (2022) 179–183, <https://doi.org/10.1016/j.jmst.2021.04.073>.
- S.Y. Lee, C.P. Kim, J.D. Aimer, U. Lienert, E. Ustundag, W.L. Johnson, Pseudo-binary phase diagram for Zr-based *in situ* β phase composites, *J. Mater. Res.* 22 (2007) 538–543, <https://doi.org/10.1557/JMR.2007.0066>.
- J.W. Qiao, S. Wang, Y. Zhang, P.K. Liaw, G.L. Chen, Large plasticity and tensile necking of Zr-based bulk-metallic-glass-matrix composites synthesized by the Bridgman solidification, *Appl. Phys. Lett.* 94 (2009), 151905, <https://doi.org/10.1063/1.3118587>.
- J.L. Cheng, G. Chen, C.T. Liu, Y. Li, Innovative approach to the design of low-cost Zr-based BMG composites with good glass formation, *Sci. Rep.* 3 (2013) 2097, <https://doi.org/10.1038/srep02097>.
- L. Zhang, R.L. Narayan, B.A. Sun, T.Y. Yan, U. Ramamurty, J. Eckert, H.F. Zhang, Cooperative shear in bulk metallic glass composites containing metastable β -Ti dendrites, *Phys. Rev. Lett.* 125 (2020), 055501, <https://doi.org/10.1103/PhysRevLett.125.055501>.
- C. Fan, C. Li, A. Inoue, V. Haas, Deformation behavior of Zr-based bulk nanocrystalline amorphous alloys, *Phys. Rev. B* 61 (2000) R3761–R3763, <https://doi.org/10.1103/PhysRevB.61.R3761>.
- Q.L. Xing, J. Eckert, W. Loser, L. Schultz, High-strength materials produced by precipitation of icosahedral quasicrystals in bulk Zr-Ti-Cu-Ni-Al amorphous alloys, *Appl. Phys. Lett.* 74 (1999) 664, <https://doi.org/10.1063/1.122980>.
- A. Inoue, W. Zhang, T. Tsurui, A.R. Yavari, A.L. Greer, Unusual room-temperature compressive plasticity in nanocrystal-toughened bulk copper-zirconium glass, *Philos. Mag. Lett.* 85 (2005) 221–229, <https://doi.org/10.1080/09500830500197724>.
- Y. Shi, M.L. Falk, A computational analysis of the deformation mechanisms of a nanocrystal-metallic glass composite, *Acta Mater.* 56 (2008) 995–1000, <https://doi.org/10.1016/j.actamat.2007.11.005>.
- D. Soppa, Y. Ritter, H. Gleiter, K. Albe, Deformation behavior of bulk and nanostructured metallic glasses studied via molecular dynamics simulations, *Phys. Rev. B* 83 (2011), <https://doi.org/10.1103/PhysRevB.83.100202>, 100202(R).
- J. Wu, Y. Pan, L. Zhang, J. Pi, Fabrication of Cu rich bulk metallic glass composites via solidification method, *Mater. Sci. Technol.* 30 (2014) 166–170, <https://doi.org/10.1179/1743284713Y.0000000329>.
- J. Eckert, A. Kübler, L. Schultz, Mechanically alloyed Zr₅₅Al₁₀Cu₃₀Ni₅ metallic glass composites containing nanocrystalline W particles, *J. Appl. Phys.* 85 (1999) 7112, <https://doi.org/10.1063/1.370519>.
- H. Choi-Yim, R.D. Conner, F. Szuets, W.L. Johnson, Processing, microstructure and properties of ductile metal particulate reinforced Zr₅₇Nb₅Al₁₀Cu_{15.4}Ni_{12.6} bulk metallic glass composites, *Acta Mater.* 50 (2002) 2737–2745, [https://doi.org/10.1016/S1359-6454\(02\)00113-1](https://doi.org/10.1016/S1359-6454(02)00113-1).
- J. Ma, C. Yang, X.D. Liu, B.S. Shang, Q.F. He, F.C. Li, T.Y. Wang, D. Wei, X. Liang, X.Y. Wu, Y.J. Wang, F. Gong, P.F. Guan, W.H. Wang, Y. Yang, Fast surface dynamics enabled cold joining of metallic glasses, *Sci. Adv.* 5 (2019) eaax7256, <https://doi.org/10.1126/sciadv.aax7256>.
- J. Ma, X.Y. Zhang, D.P. Wang, D.Q. Zhao, D.W. Ding, K. Liu, W.H. Wang, Superhydrophobic metallic glass surface with superior mechanical stability and corrosion resistance, *Appl. Phys. Lett.* 104 (2014), 173701, <https://doi.org/10.1063/1.4874275>.
- H. Zhao, F. Sun, X. Li, Y. Ding, Y.Q. Yan, X. Tong, J. Ma, H.B. Ke, W.H. Wang, Ultra-stability of metallic supercooled liquid induced by vibration, *Scr. Mater.* 194 (2021), 113606, <https://doi.org/10.1016/j.scriptamat.2020.10.048>.
- Z. Li, Z. Huang, F. Sun, X. Li, J. Ma, Forming of metallic glasses: mechanisms and processes, *Mater. Today Adv.* 7 (2020), 100077, <https://doi.org/10.1016/j.mtadv.2020.100077>.
- X. Li, X. Liang, Z. Zhang, J. Ma, J. Shen, Cold joining to fabricate large size metallic glasses by the ultrasonic vibrations, *Scr. Mater.* 185 (2020) 100–104, <https://doi.org/10.1016/j.scriptamat.2020.03.059>.
- X. Li, D. Wei, J.Y. Zhang, X.D. Liu, Z. Li, T.Y. Wang, Q.F. He, Y.J. Wang, J. Ma, W. H. Wang, Y. Yang, Ultrasonic plasticity of metallic glass near room temperature, *Appl. Mater. Today* 21 (2020), 100866, <https://doi.org/10.1016/j.apmt.2020.100866>.
- H.E. Kissinger, Reaction kinetics in differential thermal analysis, *Anal. Chem.* 29 (1957) 1702–1706, <https://doi.org/10.1021/ac60131a045>.
- C. Fan, A. Inoue, Ductility of bulk nanocrystalline composites and metallic glasses at room temperature, *Appl. Phys. Lett.* 77 (2000) 46, <https://doi.org/10.1063/1.126872>.
- B. Yang, M.L. Morrison, P.K. Liaw, R.A. Buchanan, G.Y. Wang, C.T. Liu, M. Denda, Dynamic evolution of nanoscale shear bands in a bulk-metallic glass, *Appl. Phys. Lett.* 86 (2005), 141904, <https://doi.org/10.1063/1.1891302>.